CONVERGENCE ANALYSIS OF C^K-GFEM APPLIED TO TWO-DIMENSIONAL ELASTOPLASTIC PROBLEMS

Andresa Freitas

Paulo de Tarso R. de Mendonça

Clovis Sperb de Barcellos

Diego Amadeu Furtado Torres

andresamtm@gmail.com

mendonca@grante.ufsc.br

barcellos@grante.ufsc.br

diego.amadeu@gmail.com

Grupo de Análise e Projeto Mecânico – GRANTE, departamento de Engenharia Mecânica, Universidade Federal de Santa Catarina, 88040-900, Florianópolis, SC, Brasil.

Abstract. *For many practical applications in engineering, a complex structure shows linear elastic behavior over large areas, but exhibits confined plasticity contained in some small critical regions. For analysis of these cases it is proposed the modeling using the C^k-GFEM. The first goal of this study is to verify the GFEM implementation for two-dimensional elastoplasticity and, after that, introduce an investigation trying to enlighten some advantages of higher-regularity partitions of unity against conventional C^0 counterparts. The enrichment is made with polynomial functions and global convergence measures are compared with analytical solutions. The irreversible response and hardening effects of the material is represented by the rate independent J_2 plasticity theory with linear isotropic hardening of material and von Mises yield criteria, being considered only monotonic loading and the kinematics of small displacements and small deformations. The present results constitute the initial step of a larger work which aims to use the C^k-GFEM in the local problem of the Global-Local GFEM framework.*

Keywords: *Generalized finite element method, smooth GFEM based approximations, Elastoplasticity, Convergence analysis.*

1 INTRODUCTION

Certain local characteristics of boundary value problems such as high gradient, singularities and discontinuities, can be successful modeled with the use of the classical generalized finite element method (C^0-GFEM), since it uses a priori knowledge about the solution of a problem in the form of enrichment functions. However, the piecewise regular partition of unit functions used by this method may not to be efficient for some kinds of problems. In this context, the C^k-GFEM, which is quite similar to C^0-GFEM, presents the high regularity of the approximation as an attractive feature, and the partition of unity property is retained. The importance of C^k-GFEM is also due to the fact that several kinematic plate models, such as Kirchhoff and Reddy, require solutions of continuity at least C^1.

Furthermore, studies have shown that GFEM has been used successfully in linear elastic fracture mechanics (Areias & Belytschko, 2005), (Belytschko, 2001), (Laborde et al., 2005). However, a real structure is a very complex body with stress states whose values based on the linear elasticity may exceed the elastic limits (Chen et al, 1988).

The goal in this paper is to compare the C^k-GFEM and C^0-GFEM performances in modeling two-dimensional problems involving elastoplastic fracture mechanics, contemplating problems with stress concentration (e.g. L-shaped), i.e. situations where the plasticized zone is confined to one or a few regions of the body. These kinds of problems are important because of the high gradient of deformation field that occurs in the boundary zone plasticized that is difficult to be represented with coarse meshes and conventional functions of FEM, and because of the ability of the approximation functions with C^k arbitrary inter-element continuity to build continuous stress fields.

The irreversible response and hardening effects of the material is represented by rate independent J_2 plasticity theory with linear isotropic hardening of material and von Mises yield criteria, being considered only monotonic loading and the kinematics of small displacements and small deformations.

The present results constitute the initial step of a larger work which aims to use the C^k-GFEM in the local problem of the Global-Local GFEM ($GFEM^{gl}$). This method combines the classic global-local FEM (technical "zooming" (Noor, 1986)) with the partition of unit structure, building enrichment functions numerically. Local boundary value problems are modeled in the neighborhood of local features such as cracks, where the solution exhibits high gradients or singularities (Kim et al., 2008). Local solutions, so-called global-local enrichment functions, are used to enrich the space of global approximation, based on the partition of unity structure. Thus, the proposed method does not depend on analytical solutions.

The $MEFG^{gl}$ procedure involves three steps:

(I) The solution of global problem, calculated on a coarse mesh, where cracks and yielding usually are not discretized.

(II) The solution of local problems, with small subdomains extracted of the global domain, is evaluated taking the global solution as boundary conditions.

(III) The solution of enriched global problem with the global-local enrichment functions, provided as the solution of the local problems.

2 GENERALIZED FINITE ELEMENT METHOD (C^0-GFEM)

The generalized finite element method (GFEM) is a combination of the standard finite element method (FEM) with concepts and techniques typical of meshless methods. This method presents an aspect of nodal enrichment that may not require refinement of the meshes, making it very attractive for various analyzes. In case of problems with complex domain it presents good results with the use of simple meshes (Strouboulis at al., 2001). Its efficacy has been shown, for example, in problems domains with complex boundaries form (Babuska et al., 2004).

The GFEM provides a mesh that is used to define a partition of unit (PU) and a domain for the numerical integration over which the enrichment of the PU functions is performed. The set of PU functions is employed to ensure the inter-elementar continuity, providing conformity of approximations that are improved by nodal enrichment strategy.

The enrichment functions are linked to the nodal points of the domain in order to improve the quality of approximation in the neighborhood of these points. Thus, one has the possibility to enrich the approximation only in a region of the problem domain, due to the compact support of PU, without mesh refinement (Duarte et al., 2000), (Barros et al., 2004). Moreover, the essential boundary conditions can be imposed exactly as in the standard FEM (Strouboulis at al., 2001).

To build the GFEM approximation functions it is considered, for example, a conventional mesh of finite elements defined by *N* nodes with coordinates $\{\boldsymbol{x}_j\}_{j=1}^{N}$ in the domain Ω. If the enrichment is performed with relation to node $\boldsymbol{x}_j$, a generic cloud $\omega_j \in \Omega$ is defined as a union of finite elements adjacent to this node. The set of the interpolation functions belonging to each element associated with the node $\boldsymbol{x}_j$, compose the function φ_j on the support of the cloud ω_j. The enrichment functions related to the node $\boldsymbol{x}_j$, are denoted by $\boldsymbol{L}_j = \{L_{j0}, L_{j1}, \dots, L_{jq}\} = \{L_{ji}\}_{i=0}^{q}$ (with $L_{j1} = 1$) and represent a set of q + 1 linearly independent functions.

Thus, the GFEM approximation functions associated to the node $\boldsymbol{x}_j$ result of the enrichment of PU, i.e., multiplying the PU function with support in the cloud ω_j by components of $\boldsymbol{L}_j$ (defined for each node $\boldsymbol{x}_j$ with support in the cloud ω_j)

$$\{\phi_{ji}\}_{i=0}^{q} = \varphi_j \{L_{ji}\}_{i=0}^{q} \text{ (no sum on } j). \tag{1}$$

The resulting approximation function ϕ_{ji} contains features of both functions, that is, the compact support of PU and the approximation feature of enrichment function. The structure of GFEM offers more freedom in the choice of approximation functions compared to the standard FEM.

The generalized global approximation for the displacement on $\Omega \in \Re^2$, denoted as $\boldsymbol{u}_h(\boldsymbol{x}) = \{u_{x_h}(\boldsymbol{x}), u_{y_h}(\boldsymbol{x})\}$ can be written as a linear combination of approximation functions associated with each node. The component u_{x_h}, for example, can be write as:

$$u_{x_h}(\boldsymbol{x}) = \sum_{j=1}^{N} \varphi_j(\boldsymbol{x}) \{u_j + \sum_{i=1}^{q_j} L_{ji}(\boldsymbol{x}) b_{ji}\} \Rightarrow u_{x_h}(\boldsymbol{x}) = \boldsymbol{\Phi}^T \underline{\boldsymbol{u}}, \tag{2}$$

where

$$\underline{\boldsymbol{u}}^T(\boldsymbol{x}) = \{u_1 \quad b_{11} \quad \cdots \quad b_{1q_j} \quad \cdots \quad u_N \quad b_{N1} \quad \cdots \quad b_{Nq_j}\}, \tag{3}$$

where u_j and b_{jq_j} are nodal parameters associated respectively with PU functions φ_j and enriched functions $\varphi_j L_{ji}$. The full set of approximation functions can be teamed in vector form as

$$\boldsymbol{\Phi}^T = \left\{\varphi_1 \quad L_{11}\varphi_1 \quad \cdots \quad L_{1q_j}\varphi_1 \quad \cdots \quad \varphi_N \quad L_{N1}\varphi_N \quad \cdots \quad L_{Nq_j}\varphi_N\right\}. \tag{4}$$

The continuity of the function $\boldsymbol{u}_h$ on the whole domain is guaranteed by the compact support of PU.

2.1 Model elasticity problem

Let a boundary value problem (BVP) defined in a linear elastic domain $\Omega \in \mathbb{R}^2$, where the strong form of equilibrium equations is given by

$$\begin{aligned} &\nabla^T\boldsymbol{\sigma} + \boldsymbol{b} = 0 && \text{em } \Omega \\ &\boldsymbol{u} = \bar{\boldsymbol{u}} && \text{em } \Gamma_D \\ &\boldsymbol{\sigma}\cdot\boldsymbol{n} = \bar{\boldsymbol{t}} && \text{em } \Gamma_N \end{aligned} \tag{5}$$

where $\boldsymbol{\sigma}$ is the vector containing the stress tensor components, $\boldsymbol{b}$ is the vector of body forces, Γ_D and Γ_N ($\Gamma_D \cap \Gamma_N = \emptyset$) denote complementary parts of the boundary $\partial\Omega$, where Dirichlet and Neumann conditions are defined respectively; $\bar{\boldsymbol{u}}$ and $\bar{\boldsymbol{t}}$ are prescribed displacements and tractions respectively, and $\boldsymbol{n}$ is the unit outward normal to Γ_N.

The variational form of this problem can be presented as:
Find $\boldsymbol{u} \in \boldsymbol{U}(\Omega)$ such that:

$$B(\boldsymbol{u},\boldsymbol{v}) = l(\boldsymbol{v}) \qquad \forall\boldsymbol{v} \in \boldsymbol{V}(\Omega),\ \text{com } \boldsymbol{u} = \bar{\boldsymbol{u}} \text{ em } \Gamma_D \tag{6}$$

where $\boldsymbol{U}(\Omega)$ and $\boldsymbol{V}(\Omega)$ are Hilbert spaces of degree 1 (standard Sobolev space of square integrable functions whose first derivatives are square integrable) defined on the domain Ω. The variational operators are defined as:

$$B(\boldsymbol{u},\boldsymbol{v}) = \iint_\Omega \boldsymbol{\epsilon}^T(\boldsymbol{v})\boldsymbol{\sigma}(\boldsymbol{u})\, l_z\, dxdy \tag{7}$$

$$l(\boldsymbol{v}) = \iint_\Omega \boldsymbol{v}^T\boldsymbol{b}\, l_z\, dxdy + \int_{\Gamma_N} \boldsymbol{v}^T\,\bar{\boldsymbol{t}}\, l_z\, ds \tag{8}$$

where $\boldsymbol{u}^T = \{u_x, u_y\}$ is the vector of displacements, $\boldsymbol{v}^T = \{v_x, v_y\}$ is the test function vector, $\boldsymbol{\epsilon}$ is the vector containing the strain tensor components, and l_z is the thickness of the elastic body (in the *z* reference direction) considered here as constant.

The Galerkin approximation in Eq. (6), similarly to FEM, results in:

$$\text{Find } \boldsymbol{u}_h \in \boldsymbol{U}_h \text{ such that: } B(\boldsymbol{u}_h,\boldsymbol{v}_h) = l(\boldsymbol{v}_h) \qquad \forall\boldsymbol{v}_h \in \boldsymbol{V}_h, \tag{9}$$

where $\boldsymbol{U}_h$ and $\boldsymbol{V}_h$ are $\boldsymbol{H}^1$ subspaces of finite dimension, wherein the first space is generated by the approximation functions and the second one is of test functions; $\boldsymbol{u}_h$ is obtained from Eq. (2) and the component v_{x_h}, for example, of the $\boldsymbol{v}_h = \left\{v_{x_h}, v_{y_h}\right\}$ is given by:

$$v_{x_h}(\boldsymbol{x}) = \sum_{j=1}^N \varphi_j(\boldsymbol{x})\left\{v_j + \sum_{i=1}^{q_j} L_{ji}(\boldsymbol{x})c_{ji}\right\} \Rightarrow v_{x_h}(\boldsymbol{x}) = \boldsymbol{\Phi}^T\underline{\boldsymbol{v}}, \tag{10}$$

where $\underline{\boldsymbol{v}}$ is a vector of nodal parameters similar to that shown in Eq. (3).

The only difficulty in this implementation is that the partition of unity and the bases of spaces of enrichment functions can be linearly dependent, so that the system of equations resulting from Eq. (9) is positive semi-definite. The linear dependence occurs when using the same kinds of PU and enrichment functions, such as polynomial functions. This problem can be avoided by careful choice of functions L_{ji} (Oden et al., 1998), constraints in PU (Melenk & Babuska, 1996), or the system can be efficiently solved by numerical strategy proposed in Duarte et al. (2000) and Strouboulis at al. (2001).

3 ARBITRARY CONTINUOUS FUNCTIONS (GFEM C^K)

C^k-GFEM is quite similar to C^0-GFEM, except that it uses finite element meshes to build an arbitrarily smooth PU (arbitrary continuity) (Duarte et al., 2005), called *C^k partition of unity based finite elements*. This method is not meshless, but preserves several attractive features of meshless approximations, such as the high regularity of approximation and partition of unity property. The C^k-GFEM is also important because several kinematic plate models, such as Kirchhoff and Reddy, require solutions of continuity at least C^1.

The PU functions can also be built as C^∞ functions only in clouds with convex support. In clouds with support not convex they are *k*-times continuously differentiable in the concave nodes, with *k* arbitrarily large, and infinitely differentiable in the rest of the domain. The technique used for the construction of C^k PU is described below.

In a conventional finite element mesh defined by *N* nodes with coordinates $\{\boldsymbol{x}_j\}_{j=1}^{N}$ in the domain Ω is considered a set of functions $W_j(\boldsymbol{x}) \subset C_0^k(\omega_j)$, with $j = 1, ..., N$, denoted by weighting functions. Each one is associated to a cloud ω_j as its compact support. Using Shepard's formula is obtained:

$$\varphi_j(\boldsymbol{x}) = \frac{W_j(\boldsymbol{x})}{\sum_{\beta(x)} W_\beta(x)}, \quad \beta(\boldsymbol{x}) \in \{\gamma : W_\gamma(\boldsymbol{x}) \neq 0\}. \tag{11}$$

It can be seen that the set $\{\varphi_j(\boldsymbol{x})\}_{j=1}^{N}$ is such that $\varphi_j(\boldsymbol{x}) \subset C_0^k(\omega_j)$, $k \geq 0$ and $\sum_{j=1}^{N} \varphi_j(\boldsymbol{x}) = 1$, $\forall\, x \in \Omega$ and whole compact subset of Ω intercepts only a finite number of supports. Therefore, $\varphi_j(x)$ is a partition of unity and its regularity depends only on the regularity of the weighting functions (Mendonça et al., 2011) constructed to ensure the continuity required. Thus, on each support appropriate C^k weighting functions are constructed and used in Shepard's formula, creating the partition of unity.

Thus, the resulting PU is at least *k*-times continuously differentiable, and the resulting approximation functions of the product of Shepard PU with the enrichment functions will have the same continuity since the enrichments are at least also C^k. Enrichment functions can be chosen as polynomial functions, harmonic, anisotropic or even functions that are part of the solution of the boundary value problem (Babuska et al., 2002; Strouboulis et al., 2000; Melenk & Babuska, 1996). It is noted that different choices of PU functions are possible (it depends on the choice of the edge functions (Mendonça et al., 2011)), leading to different kinds of approximation functions. An example of the edge function is showed in the section 3.1.

The building of weighting functions occurs differently depending on their supports convex or not convex.

3.1 Weighting function with convex support

The weighting functions with convex support can be built from the product of the *cloud edge functions* $\varepsilon_{j,n}[\xi_n(\boldsymbol{x})]$ associated with the cloud ω_j and defined for each edge *n* of the cloud. These functions vanish smoothly when approaching the edges and becoming greater than zero inside the cloud. All edge functions $\varepsilon_{j,n}[\xi_n(\boldsymbol{x})]$ are built to have the same value at node $\boldsymbol{x}_j$ of the cloud ω_j, where $\xi_n(\boldsymbol{x}) = \boldsymbol{n}_n \cdot (\boldsymbol{x} - \mathbf{b}_n)$ is the distance between the position $\boldsymbol{x}$ and the edge *n*, $\mathbf{b}_n$ is the edge midpoint, and $\boldsymbol{n}_n$ the normal vector to the edge directed into the cloud.

The edge functions must be at least C^k continuity, $k \geq 0$, necessary for the construction of PU. Therefore, the C^k weighting function which also vanishes on the boundary of the cloud and greater than zero in its interior is constructed from the edge functions $\varepsilon_{j,n}(\boldsymbol{x}_j)$ as follows:

$$W_j(\boldsymbol{x}) = \prod_{n=1}^{M_j} \varepsilon_{j,n}(\xi_n), \tag{12}$$

where M_j is the number of edge functions to the cloud ω_j. It is important to prevent edge functions vary greatly from cloud to cloud, because numerical experiments show it is important to have functions with similar maximum values for all edges associated with a given node of the cloud.

A kind of edge function is the polynomial of degree *p*, $p \geq k+1$, such that the function and its *k* first normal derivatives approach zero when they reach their edge *n*. They are given by

$$\varepsilon_{j,n}[\xi_n(\boldsymbol{x})] = \begin{cases} \left(\xi_n / h_{j,n}\right)^p & \text{if } \xi_n > 0 \\ 0 & \text{otherwise} \end{cases}, \tag{13}$$

where $h_{j,n}$ is the normal distance from node *j* to the edge *n*.

Another kind of edge function is the exponential with unitary value at node of the cloud and decay rate controlled by a parameter $\beta = \varepsilon_{j,n}\left[\frac{h_{j,n}}{2}\right] / \varepsilon_{j,n}\left[h_{j,n}\right]$. For these two conditions, one can use the following function edge (Barcellos et al., 2009):

$$\varepsilon_{j,n}[\xi_n(\boldsymbol{x})] = \begin{cases} A e^{-(\xi_n / B)^{-\gamma}} & \text{if } \xi_n > 0 \\ 0 & \text{otherwise} \end{cases}, \tag{14}$$

where $B = h_{j,n}\left(\frac{log_e \beta}{1-2\gamma}\right)^{\frac{1}{\gamma}}$ and β and γ are positive arbitrary constants. However, numerical experiments have shown that the most appropriate values are $\beta = 0.3$ and $\gamma = 0.6$, as suggested by Duarte et al. (2006) and Torres (2012). Therefore, at cloud node the function has the value

$$\varepsilon_{j,n}\left[\xi_n\left(x_j\right)\right] = A e^{-\left(\frac{1-2\gamma}{log_e \beta}\right)^{-1}} \tag{15}$$

which is the same for every edge n of the cloud ω_j and imposing the constraint $\varepsilon_{j,n}\left[\xi_n\left(\boldsymbol{x}_j\right)\right] = 1$, one gets $A = e^{-\left(\frac{1-2\gamma}{log_e \beta}\right)^{-1}}$.

For convex supports this exponential edge function leads to weighting functions C^∞ and, therefore, to C^∞ PU.

4 TWO-DIMENSIONAL PLASTICITY

This section presents the equations that govern the classical plasticity in the two-dimensional context, which can be found in Chen (1988), Simo & Hughes (1998) and Souza Neto et al. (2008).

The formulation adopted is based on the classical rate independent J_2 flow theory for small strain. Its main features are: von Mises yield criteria, linear isotropic hardening of material, hypothesis of associativity to the hardening law and normality rule for plastic flow. The Newton-Raphson was the iterative and incremental scheme adopted.

Initially the isotropic hardening will be used, however, kinematic hardening and cohesion models can easily be introduced to the algorithm. The plastic flow is regarded as an irreversible process and is characterized in terms of the history of the following variables: strain tensor $\boldsymbol{\epsilon}$, plastic strain tensor $\boldsymbol{\epsilon}^p$ and isotropic hardening internal variable α, related to the evolution of plastic deformation.

Considering the additive decomposition of the total strain tensor $\boldsymbol{\epsilon} = \boldsymbol{\epsilon}^e + \boldsymbol{\epsilon}^p$, the isotropic linear elastic constitutive tensor $\mathbf{C}$, the deviatoric stress tensor $\boldsymbol{s}$ and the yield stress σ_y, the equations that govern the model are:

1) elastic stress-strain relationship: $\boldsymbol{\sigma} = \mathbf{C}[\boldsymbol{\epsilon} - \boldsymbol{\epsilon}^p]$;

2) von Mises yield criterion: $f = \sqrt{\frac{3}{2}}\|\boldsymbol{s}\| - (\sigma_y + q) \leq 0$, where $q = H'\alpha$ and H' is the modulus plastic of isotropic linear hardening;

3) flow rule: $\dot{\boldsymbol{\epsilon}}^p = \gamma\partial_\sigma f = \gamma\sqrt{\frac{3}{2}}\underline{\boldsymbol{n}}$, where $\underline{\boldsymbol{n}} = \frac{\boldsymbol{s}}{\|\boldsymbol{s}\|}$;

4) hardening law: $\dot{\alpha} = \gamma\partial_q f = \gamma$;

5) accumulated plastic deformation rate: $\dot{\boldsymbol{\epsilon}}_{ac}^p = \dot{\alpha}$;

6) Kuhn-Tucker complementary conditions: $\gamma \geq 0$, $f(\boldsymbol{\sigma}, q) \leq 0$, $\gamma f = 0$;

7) consistency condition: $\gamma\dot{f}(\boldsymbol{\sigma}, q) = 0$ (se $f(\boldsymbol{\sigma}, q) = 0$), where $\dot{f}$ is the yield function rate.

The parameter $\gamma \geq 0$ is a nonnegative function, called *consistency parameter*, which represents the plastic flow rate satisfies the Kuhn-Tucker and consistency conditions.

5 NUMERICAL RESULTS

In this section, two numerical experiments are conducted. The goal is to compare the C^k-GFEM and C^0-GFEM performances by two-dimensional elastoplastic problems. The formulation was numerically implemented considering regular and uniform domain in which only convex clouds occur. The domain was partitioned in triangular elements with three nodes and straight edges. Thus, in the implementation of the C^k-GFEM was used the PU with continuity C^∞ on the whole domain, generating stress approximations with inter-element continuity. The enrichment is made with polynomial functions of degrees p =1 to 4. The integration quadrature applied in the elements was Wandzura's symmetric quadrature in triangles (Wandzura & Xiao, 2003) with 175 points. The same quadrature was used by the C^k-GFEM and C^0-GFEM for comparative purposes. For integrations in the Neumann boundary we used the Gauss-Legendre quadrature with 25 points, for each elementary edge. The irreversible response and hardening effects of the material is represented by the rate independent J_2 plasticity theory with linear isotropic hardening of material and von Mises yield criteria. It is considered only monotonic loading and the kinematics of small displacements and small deformations. The entire computational implementation was done via user code using the MATLAB® 10. The program used for this simulation was built from C^k-GFEM program for linear elastic analysis, developed by Torres (2012) during their thesis development. Internally pressurized cylinder

The first example is the simulation of behavior of a long thick-walled cylinder subjected to a gradually increasing internal pressure. The dimensions of the problem, the material parameters and the finite element mesh adopted are shown in Fig. 1. The cylinder is discretized by 64 axisymmetric elements. The maximum pressure, P, used to this problem was 0.18 GPa. Nine uniform pseudo time steps were used for incremental analysis.

The aim of this problem is to verify the C^k-GFEM and C^k-GFEM implementations in elastoplastic analysis. The numerical solutions obtained were compared with the analytical solution of Hill (1950).

Figure 2 shows the radial displacement at outer face of the cylinder versus applied pressure computed by the C^0-GFEM and C^k-GFEM. Figure 3 shows the norm of the relative error of the radial displacement at outer face versus degrees of freedom obtained via C^0-GFEM and C^k-GFEM. These values are presented in the Table 1 for b = 1, 2, 3 and 4, that represents the polynomial degree of reproducibility of the proposed GFEM approximation subspace. The respective values of b for specific values of degrees of freedom also are shown in the Table 1. In this case, $b = p + 1$ to C^0 PU and $b = p$ to C^k PU, where p is the degree of the polynomial enrichment, as suggested in Mendonça et al. (2011).

The relative error of the radial displacement is given by $e_r = \frac{\boldsymbol{u}_{ex} - \boldsymbol{u}_{ap}}{\boldsymbol{u}_{ex}}$, where $\boldsymbol{u}_{ex}$ and $\boldsymbol{u}_{ap}$ are the exact and approximated displacements, respectively.

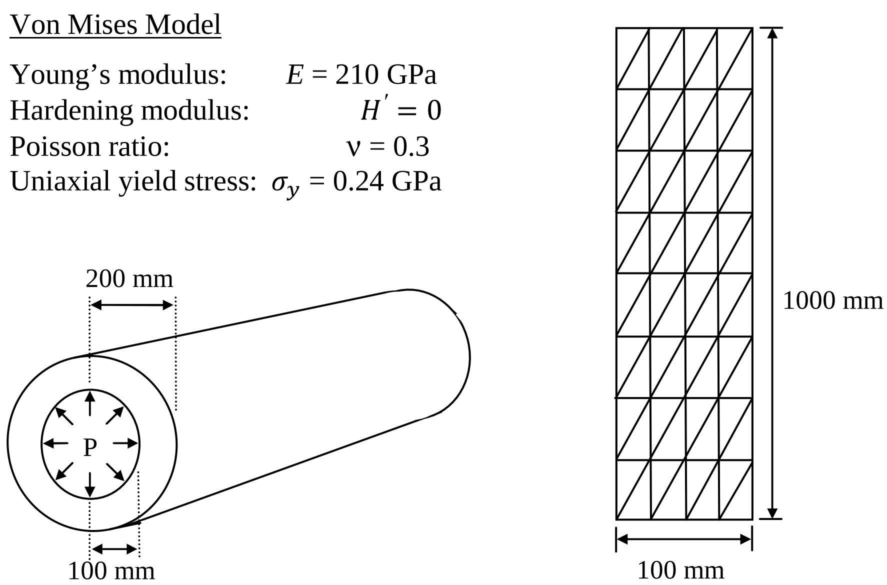

Figura 1: Internally pressurized cylinder. Material properties and finite element mesh adopted.

The C^0-GFEM and C^k-GFEM results are close to the analytical value and exhibit similar errors for the same values of b (see Table 1). As expected, the worst values of the approximations of displacement occur for b = 1. According to Fig. 2, the approximation of the displacement worsens from the yielding pressure, 0.103 GPa according to the analytical solution (Souza Neto et al., 2008), for b = 1. This suggests that for this problem (choice of mesh, PU, enrichment function) both methods do not approach well the plasticized solution when b = 1.

The circumferential stress obtained at integration points for P = 0.1 GPa (elastic solution) and P = 0.18 GPa (elastoplastic solution) are plotted for b = 2, 3 and 4 in Fig. 4 and Fig. 5 respectively, together with Hill's solution. The C^0-GFEM and C^k-GFEM results are very close to the analytical solution. The worst results occur for C^0-GFEM when b = 2, where p = 1. For the complete loading in case of P = 0.18 GPa, the plastic front reaches approximately

159.79 mm (radius of plasticization analytic). The transition from elastic to plastic zone can be visualized by a change in slope of the curve shown in Fig. 5.

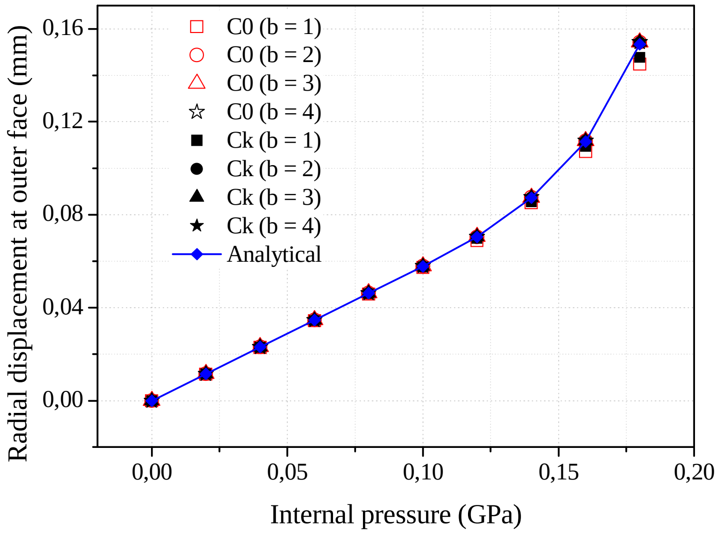

Figure 2. Radial displacement versus increasing pressure for the problem of Fig. 1.

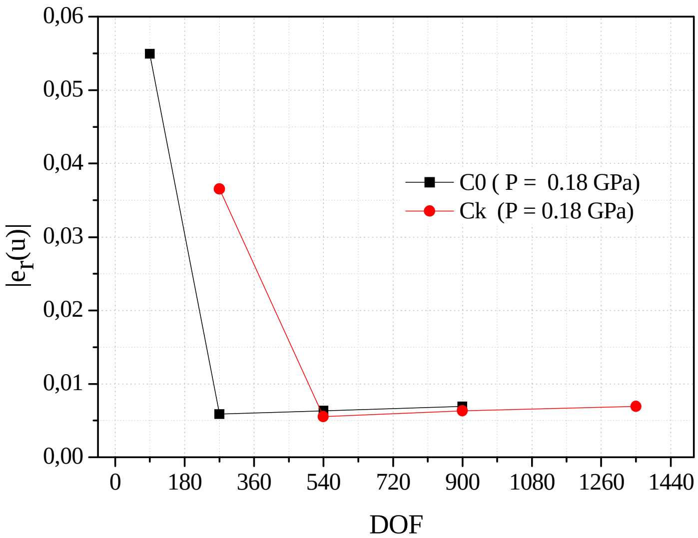

Figure 3. Norm of relative error for the radial displacement at outer face versus degrees of freedom for the problem of Fig. 1.

Table 1. Error values for the radial displacement considering different degrees b for the problem of Fig. 1.

	C^0-GFEM		C^k-GFEM	
DOF	b	$\|e_r(u)\|$	b	$\|e_r(u)\|$
90	1	0.05492 (5.49%)		
270	2	0.005871 (0.58%)	1	0.03653 (3.65%)
540	3	0.006327 (0.63%)	2	0.005545 (0.55%)
900	4	0.006915 (0.69%)	3	0.006337 (0.63%)
1350			4	0.006915 (0.69%)

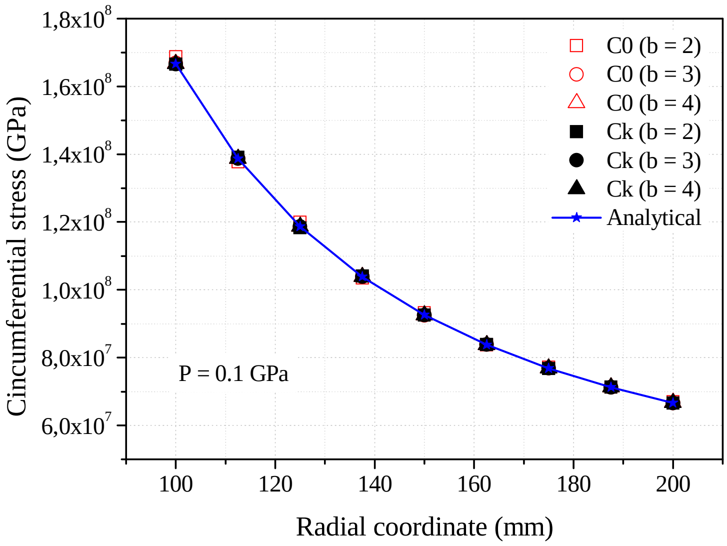

Figure 4. Circumferential stress versus radial coordinate to P = 0.1 GPa (elastic solution) for the problem of Fig. 1.

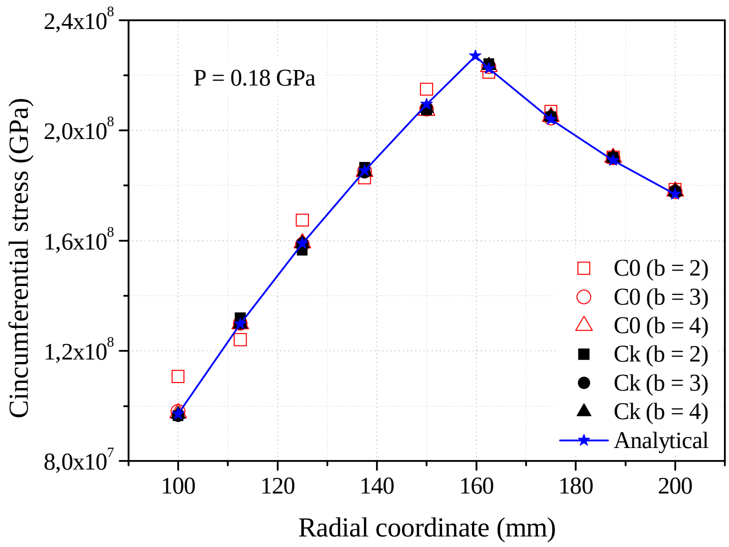

Figure 5. Circumferential stress versus radial coordinate to P = 0.18 GPa (elastoplastic solution) for the problem of Fig. 1.

5.1 L-shaped domain

The L-shaped domain is a classic problem in the theory of elasticity for which an analytical solution is known (Szabo & Babuska, 2011). However, an elastoplastic version of this is considered herein aiming to verify the evolution of a process zone at the reentrant vertex neighborhood. The loading used in this example is correspondent to Mode I opening. The analysis is carried out assuming plane strain conditions. The domain of the problem is discretized by 96 elements. The dimensions, material parameters and the finite element mesh used are shown in Fig. 6. Ten uniform pseudo time steps was used for incremental analysis. Surface forces applied on the edges AB, BC, EF and EF have been calculated according to the stress components corresponding to the term of Mode I the asymptotic expansion of the displacement field (Szabo & Babuska, 2011)

$$\sigma_x = a_1\lambda_1 r^{\lambda_1-1}\left[\left(2 - Q_1(\lambda_1+1)\right)cos(\lambda_1-1)\theta - (\lambda_1-1)cos(\lambda_1-3)\theta\right]$$

$$\sigma_y = a_1\lambda_1 r^{\lambda_1-1}\left[\left(2 + Q_1(\lambda_1+1)\right)cos(\lambda_1-1)\theta - (\lambda_1-1)cos(\lambda_1-3)\theta\right]$$

$$\tau_{xy} = a_1\lambda_1 r^{\lambda_1-1}\left[\left((\lambda_1-1)\right)sin(\lambda_1-3)\theta + Q_1(\lambda_1+1)sin(\lambda_1-1)\theta\right]$$

where $Q_1 = 0.543075579$, $\lambda_1 = 0.544483737$ and a_1 is a arbitrary real number, considered here as $a_1 = 1.0$. The force applied to this problem was multiplied by constant c = 2500.

Von Mises Model

Young's modulus: E = 210 GPa
Hardening modulus: H' = 10.5 GPa
Poisson ratio: ν = 0.3

Uniaxial yield stress: σ_y = 620 MPa
Domain dimension: a = 100 mm
Thickness constant and unitary: l_z = 1 mm

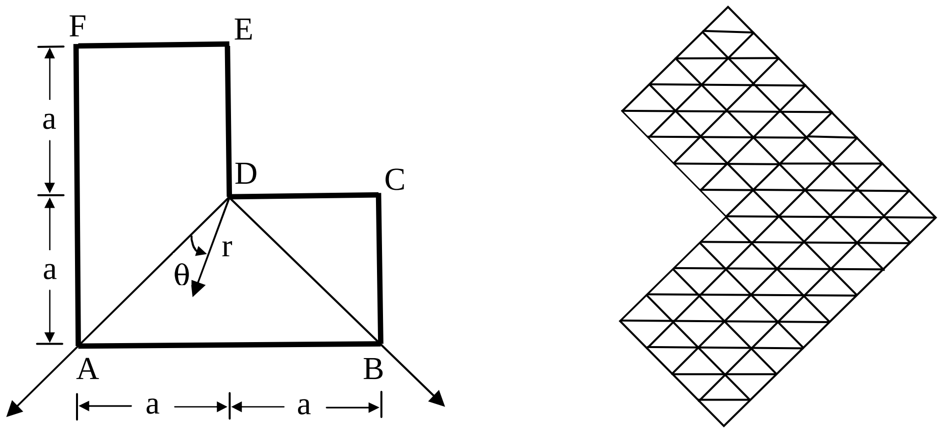

Figure 6. L-shaped domain. Material properties and finite element mesh.

The strain energy, $\mathrm{U}(\boldsymbol{u}) = \frac{1}{2}\iint_{\Omega} \boldsymbol{\epsilon}^T(\boldsymbol{u})\boldsymbol{\sigma}(\boldsymbol{u})\, l_z\, dxdy$, is used as global convergence measure to compare the elastoplastic solution to that of the elastic problems, checking numerical implementation. According Rice & Rosengren (1968), crack problems result in the same order of singularity in the product of stress and strain for both elastic and plastic cases. Thus, we suppose that the integrating of the strain energy keeps the same relationship of singularity for both elastic and plastic problems.

Table 2 shows values of the strain energy for b = 4 obtained by C^k-GFEM for approximated elastic end plastic solutions for c = 1000 e 2500. The values are compared with the analytical solution. The table indicates that the approximated strain energy values for the plastic solutions are greater than the elastic solutions; and the approximated elastic solutions are lower than the analytical solution. The approximated plastic solution is closer to the analytical solution for c = 1000. A reason for this is that the applied loading is inherent of the elastic problem, thus, for a greater plasticized zone, the difference between these strain energy values will be greater, since the applied surface load distribution does not correspond to the plasticity exact solution once such solution is unknown.

Table 3 shows values of the strain energy obtained by the C^k-GFEM and C^0-GFEM for b = 1, 2, 3 and 4 and c = 2500. We can see that these values are close to the analytical solution, considering a considerable plasticized zone (see Fig. 7).

Table 2. Values of the strain energy obtained by the C^k-GFEM for *b* = 4 and *c* = 1000 and *c* =2500, for the problem of Fig. 6.

c	Solution	$U(\boldsymbol{u})$
1000	Analytical elastic	$2.9812x10^3$
	Approximated elastic	$2.9077x10^3$
	Approximated plastic	$2.9159x10^3$
2500	Analytical elastic	$1.8626x10^4$
	Approximated elastic	$1.8173x10^4$
	Approximated plastic	$2.0736x10^4$

Table 3. Values of the strain energy for b = 1, 2, 3 and 4 and c = 2500 for the problem of Fig. 6.

	$U(\boldsymbol{u})$				Analytical elastic solution
b	1	2	3	4	-
C^k-GFEM	$1.8077x10^4$	$1.9814x10^4$	$2.0446x10^4$	$2.0736x10^4$	$1.8626x10^4$
C^0-GFEM	$1.7645x10^4$	$2.0172x10^4$	$2.085x10^4$	$2.1270x10^4$	$1.8626x10^4$

Table 4 lists the number of iterations in the Newton-Raphson scheme required in each loading step obtained by C^0-GFEM and C^k-GFEM. The results are showed for *b* = 1, 2, 3 and 4. The table indicates that the total numbers of iterations required for the two approaches are almost the same. The respective numbers of degrees of freedom used in C^0-GFEM and C^k-GFEM analyses for different values of *b* are shown in Table 5.

The process zone geometry is identified in Figure 7 that shows the points of integration distribution for which the yield condition was reached on L-shaped domain for *b* =1, 2, 3, 4 for the maximum loading level. This figure compares the C^k-GFEM and C^0-GFEM performances considering the high gradient of deformation field that occurs in the zone plasticized. The results suggest the ability of the approximation functions with arbitrary inter-element continuity to represent the zone plasticized.

Table 4. Number of iterations required at each loading step for *b* = 1, 2, 3 and 4.

	Number of iterations							
b	**1**		**2**		**3**		**4**	
Load step	**C^0-GFEM**	**C^k-GFEM**	**C^0-GFEM**	**C^k-GFEM**	**C^0-GFEM**	**C^k-GFEM**	**C^0-GFEM**	**C^k-GFEM**
1	**1**	**1**	**1**	**1**	**1**	**1**	**1**	**1**
2	**1**	**1**	**1**	**1**	**1**	**1**	**1**	**1**
3	**1**	**1**	**1**	**1**	**3**	**1**	**4**	**3**
4	**1**	**1**	**3**	**2**	**4**	**4**	**4**	**4**
5	**1**	**3**	**4**	**4**	**4**	**5**	**4**	**5**
6	**1**	**5**	**4**	**5**	**5**	**8**	**4**	**5**
7	**6**	**5**	**5**	**5**	**5**	**7**	**5**	**5**
8	**5**	**5**	**5**	**5**	**5**	**6**	**6**	**5**
9	**6**	**6**	**5**	**5**	**7**	**6**	**5**	**6**
10	**6**	**6**	**5**	**5**	**6**	**6**	**6**	**6**
Total	**29**	**34**	**34**	**34**	**41**	**45**	**40**	**41**

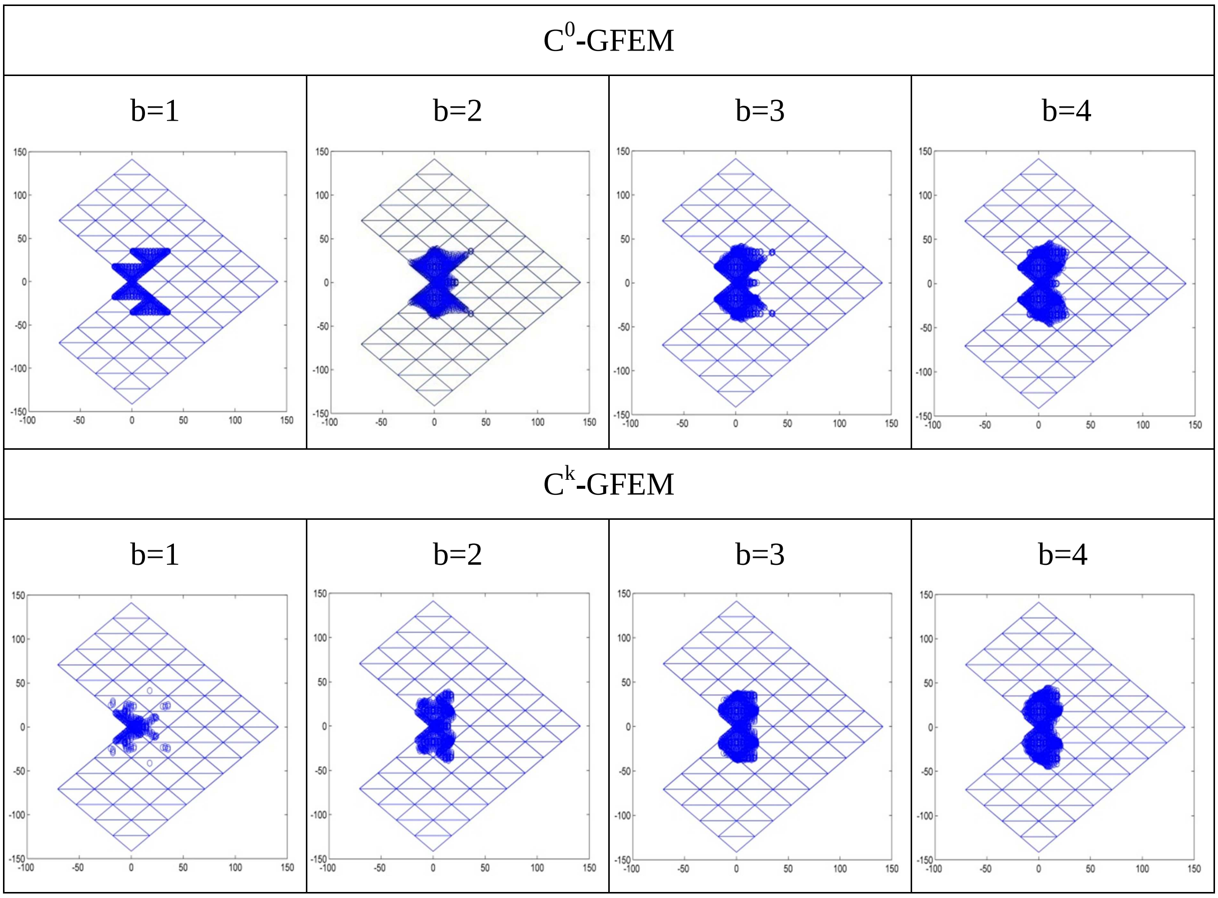

Figure 7. Locus of integration points for which the yield condition was reached, for the problem of Fig. 6.

Table 5. Numbers of degrees of freedom for *b* = 1, 2, 3 and 4.

	C^0-GFEM	C^k-GFEM	C^0-GFEM	C^k-GFEM	C^0-GFEM	C^k-GFEM	C^0-GFEM	C^k-GFEM
b	**1**		**2**		**3**		**4**	
DOF	**130**	**390**	**390**	**780**	**780**	**1300**	**1300**	**1950**

6 CONCLUSION

The aim of this study was to verify the GFEM implementation for two-dimensional elastoplasticity and, after that, compare through numerical experiments the C^k-GFEM and C^0-GFEM performances in problems with confined plasticity based on J_2 plasticity theory. For the two problems analyzed such comparison was performed using local and global convergence measures, respectively. The results presented for the pressurized cylinder problem show that the quality of the stress is almost the same for both C^0-GFEM and C^k-GFEM, for the same degree of the approximation *b*. That is expected considering that this problem is essentially one-dimensional. On the other hand, the results presented for the L-Shaped problem suggest that the C^k-GFEM represents better the plasticized region when compared with C^0-GFEM. These are the first exploratory results that constitute the initial step of a larger work which aims to use the C^k-GFEM in the local problem of the Global-Local GFEM ($GFEM^{gl}$). One of the steps of future research is to keep the process of checking of the L-shaped problem, where another investigations will be even performed. The effect of different meshes in the solution of the problem and comparing the result with that found via ANSYS® (2010) with a very refined mesh, are some most immediate investigations to the work.

REFERENCES

ANSYS® (2010) User's manual. ANSYS Inc, USA.

Areias, P. M. A. & Belytschko, T., 2005. Analysis of three-dimensional crack initiation and propagation using the extended finite element method. *International Journal for Numerical Methods in Engineering*, v. 63, pp. 760-788**.**

Babuska, I., Banerjee, U. & Osborn, J.E., 2002. On principles for a selection of shape functions Generalized Finite Element Method. *Computer Methods in Applied Mechanics and Engineering*, v. 191, pp. 5595-5629.

Babuska, I., Banerjee, U. & Osborn, J.E., 2004. Generalized finite element methods - main ideas, results and perspective. *International Journal of Computational Methods*, v. 1, n. 1, pp. 67-103.

Barcellos, C. S., Mendonça, P. T. R. & Duarte, C. A., 2009. A C^k continuous generalized finite element formulation applied to laminated Kirchhoff plate model. *Computational Mechanics*, v. 44, p. 377-393.

Barros, F. B., Proença, S. P. B. & Barcellos, C. S. de, 2004. Generalized finite element method in structural nonlinear analysis - a p-adaptative strategy. *Computational Mechanics*, v. 33, pp. 95-107.

Belytschko, T., Moës, N., Usui, S. & Parimi,C., 2001. Arbitrary discontinuities in finite elements. *International Journal for Numerical Methods in Engineering*, v. 50, pp. 993-1013**.**

Chen, W. F. & HAN, D. J., 1988. *Plasticity for structural engineers*. Springer-Verlag, New York.

Duarte, C. A., Babuska, I. & Oden, J. T., 2000. Generalized finite element method for three-dimensional structural mechanics problems. *Computer Structures*, v. 77, pp. 215-232.

Duarte, C. A., Kim, D.J., Quaresma, D. M., 2006. Arbitrarily smooth generalized finite element approximations. *Computer Methods in Applied Mechanics and Engineering*, v. 196, pp. 33-56.

Duarte, C. A., Migliano, C. A. & Baker, E. B., 2005. *A technique to combine meshfree and finite element-based partition of unit approximations*. (Department of Civil and Environmental Engineering - University of Illinois at Urbana - Champaign) Structural Research Series 638.

Hill, R., 1950. *The mathematical theory of plasticity*. Oxford University Press, London.

Kim, D. J, Duarte, C. A. & Pereira, J. P, 2008. Analysis of interacting cracks using the generalized finite element method with global-local enrichment functions.

Laborde, P., Pommier J., Renard Y. & Salaün, M., 2005. High-order extended finite element method for cracked domains. *International Journal for Numerical Methods in Engineering*, v. 64, pp. 354-381.

Melenk, J.M. & Babuska, I., 1996. The partition of unity finite element method: Basic theory and applications. *Computer Methods in Applied Mechanics and Engineering*, v. 139, p. 289-314.

Mendonça, P. T. R., Barcellos, C. S. & Torres, D. A., 2011. Analysis of anisotropic Mindlin plate model by continuous and non-continuous GFEM. *Finite elements in Analysis and Design*, n. 47, p. 698-717.

Noor, A. K., 1986. Global-local methodologies and their application to nonlinear analysis. *Finite Elements in Analysis and Design*, v.2, pp. 333-346.

Oden, J. T., Duarte, C. A. M. & Zienkiewicz, O. C., 1998. A new cloud-based hp finite element method. *Computer Methods in Applied Mechanics and Engineering*, v.153, p. 117-126.

Rice, J. R. & Rosengren G. F., 1968. Plane strain deformation near a crack tip in a power-law hardening material. *Journal of the Mechanics and Physics of Solids*, v. 16, p. 1-12.

Simo, J. C. & Hughes T. J. R., 1998. *Computational Inelasticity*. Springer-Verlag, New York.

Souza Neto, E. A., Peric, D. & Owen, D. R., 2008. *Computational Methods for Plasticity: Theory and Applications*. 1. ed. John Wiley & Sons.

Strouboulis T., Copps, K. & Babuska, I., 2001. The generalized finite element method. *Computer Methods in Applied Mechanics and Engineering*, v. 190, p. 4081- 4193.

Strouboulis, T., Babuska, I. & Copps, K., 2000. The design and analysis of generalized finite element method. *Computer Methods in Applied Mechanics and Enginnering*, v. 181, p. 43-69.

Szabo , B. & Babuska, I., 2011. *Introduction to finite element analysis: formulation, verification and validation.* Chichester, United Kingdon: Wiley, 372 p.

Torres, D. A. F., 2012. *Contribuições sobre a utilização de funções de aproximação contínuas no método generalizado de elementos finitos: Avaliação em mecânica da fratura*. Tese, Universidade Federal de Santa Catarina.

Wandzura, S. & Xiao, H., 2003. Symmetric quadrature rules on a triangle. *Computers and Mathematics with Applications*, v. 45, p. 1829 – 1840.